Article

On using oscillating time-dependent restraints in MD simulation

Bettina Keller[a], Markus Christen[a], Chris Oostenbrink[b] & Wilfred F. van Gunsteren[a],*
[a]*Laboratorium für Physikalische Chemie, ETH Zürich, Zürich, CH-8093, Switzerland;* [b]*Computational Medicinal Chemistry and Toxicology, Department of Pharmacochemistry, Vrije Universiteit, De Boelelaan 1083, 1081 HV, Amsterdam, The Netherlands*

Abstract

The use of time-dependent restraints in molecular simulation in order to generate a conformational ensemble for molecules that is in accordance with measured ensemble averages for particular observable quantities is investigated. Using a model system consisting of liquid butane and the cyclic peptide antamanide the reproduction of particular average [3]*J*-coupling constant values in a molecular dynamics simulation is analysed. It is shown that the multiple-valuedness and the sizeable gradients of the Karplus curve relating [3]*J*-coupling constants measured in NMR experiments to the corresponding torsional-angle values cause severe problems when trying to restrain a [3]*J*-coupling constant to a value close to the extrema of the Karplus curve. The introduction of a factor oscillating with time into the restraining penalty function alleviates this problem and enhances the restrained conformational sampling.

Introduction

Our knowledge of the structural characteristics of biomolecules such as proteins, saccharides, nucleic acids and lipids stems from the interpretation of spectroscopic or diffraction measurements. These measurements deliver time- and spatial (over different molecules) averages of particular observable quantities, for example [3]*J*-coupling values, Nuclear Overhauser Enhancement (NOE) intensities or dipolar coupling values from NMR spectroscopy or structure factor amplitudes from X-ray or neutron diffraction. Because these observable quantities generally depend in a non-linear manner on the 3-dimensional structure or conformation of a biomolecule, it is not straightforward and often impossible to derive the probability distribution of molecular conformations from

such experiments (Hendrickson, 1981; Case, 1998; van Gunsteren et al., 1999). Only if this conformational distribution is dominated by a particular conformation, a "structure" may be derived from the experimental data. If the conformational distribution is characterized by two or more conformations of comparable probability, "structure" determination becomes difficult. The experimentally measured value q^{obs} of a quantity $q(\mathbf{r})$ that depends on the conformation $\mathbf{r}$ will result from averaging the q-values corresponding to the dominant conformations, i.e. $q^{obs} = \langle q(\mathbf{r}) \rangle_{\mathbf{r}}$. If the observable $q(\mathbf{r})$ depends non-linearly upon conformation $\mathbf{r}$ or if the conformational distribution is not uni-modal (Figure 1), the conformation $\mathbf{r}_{\langle q \rangle}$ that corresponds to the average q-value $\langle q \rangle$ may have a very low probability $P(\mathbf{r})$. Using such measured average q-values in single structure determination may then lead to unlikely or high-energy biomolecular structures or structures of particular parts of

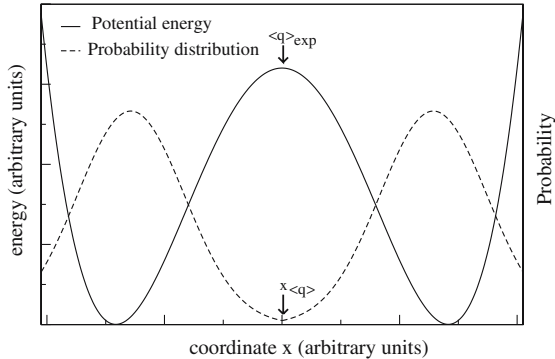*To whom correspondence should be addressed. E-mail: wfvgn@igc.phys.chem.ethz.ch

Figure 1. Energy and conformational probability along a coordinate. *solid line:* double-well potential; *dashed line:* corresponding probability distribution; $x_{\langle q \rangle}$ coordinate that corresponds to the experimentally measured value $\langle q \rangle_{\mathrm{exp}}$ of a quantity or observable q (for a linear dependence of q on x).

a molecule (Jardetzky, 1980; van Gunsteren et al., 1999).

Computer simulation of the motion of a biomolecular system produces a trajectory or an ensemble of molecular conformations, which can be used to interpret the available experimental data (van Gunsteren and Berendsen, 1990; Karplus and McCammon, 2002; Norberg and Nilsson, 2003). Trajectory or ensemble averages of observable quantities can be calculated and compared to the measured values. If these agree with each other, the simulated conformational ensemble may be considered to be realistic and it may be used to calculate quantities that are not or even cannot be observed experimentally. In this way computer simulation complements the measurement. If the molecular model and force field used in the simulation would be infinitely accurate and the simulation could be made infinitely long, one would even not need to perform experiments. However, this state of affairs is still beyond the horizon for larger biomolecular systems. The accuracy of current biomolecular force fields is limited due to the intrinsic averaging over the omitted (electronic) degrees of freedom. It only incorporates their mean effect. Secondly, molecular dynamics (MD) simulations nowadays cover the nanosecond time scale, which may not offer sufficient sampling to calculate averages of quantities that are measured over much larger (milliseconds) time scales. To make up for these deficiencies of computer simulation one can resort to imposing the experimentally observed average

value q^{obs} as a boundary condition onto the simulation: a trajectory or ensemble of configurations is to be generated for which the relation

$$\langle q(\mathbf{r}) \rangle_{\mathbf{r}} = q^{\mathrm{obs}} \tag{1}$$

holds. In other words, given a potential energy function $V(\mathbf{r})$ and given equations of motion or a sampling method such as Monte Carlo sampling for generating a Boltzmann ensemble, their form or parameters should be modified such as to drive the average $\langle q(\mathbf{r}) \rangle_{\mathbf{r}}$ to agree with q^{obs}. There are at least five distinct approaches to restrain the motion or the conformational distribution along the degrees of freedom $\mathbf{r}$ such that (1) is satisfied (van Gunsteren et al., 1996b): (i) constraint methods, (ii) penalty function methods, (iii) extended system methods, (iv) weak coupling methods, and (v) stochastic methods. Since the penalty function method is most widely used in structure determination based on NMR spectroscopic or X-ray diffraction data, only this technique will be considered here.

The average $\langle q(\mathbf{r}) \rangle_{\mathbf{r}}$ can be restrained to the value q^{obs} by adding a restraining or penalty function term

$$V^{qr}\bigl(\langle q(\mathbf{r}) \rangle_{\mathbf{r}}; q^{\mathrm{obs}}\bigr) \tag{2}$$

to the physical interaction function $V^{\mathrm{phys}}(\mathbf{r})$

$$V(\mathbf{r}) = V^{\mathrm{phys}}(\mathbf{r}) + V^{qr}\bigl(\langle q(\mathbf{r}) \rangle_{\mathbf{r}}; q^{\mathrm{obs}}\bigr). \tag{3}$$

The resulting function $V(\mathbf{r})$ is then used in the equations of motion or sampling procedure. The restraining term V^{qr} should be chosen such that its value increases the more $\langle q(\mathbf{r}) \rangle_{\mathbf{r}}$ deviates from q^{obs} (Kaptein et al., 1985), e.g.

$$
\begin{aligned}
V^{qr}&\bigl(\langle q(\mathbf{r}) \rangle_{\mathbf{r}},\ q^{\mathrm{obs}}\bigr) = 0 \\
&\text{if } \langle q(\mathbf{r}) \rangle_{\mathbf{r}} \leq q^{\mathrm{obs}} \\
&= \frac{1}{2} K^{qr}\bigl(\langle q(\mathbf{r}) \rangle_{\mathbf{r}} - q^{\mathrm{obs}}\bigr)^2 \\
&\text{if } q^{\mathrm{obs}} \leq \langle q(\mathbf{r}) \rangle_{\mathbf{r}} \leq q^{\mathrm{obs}} + \Delta q \\
&= K^{qr}\left(\langle q(\mathbf{r}) \rangle_{\mathbf{r}} - q^{\mathrm{obs}} - \frac{1}{2}\Delta q\right)\Delta q \\
&\text{if } q^{\mathrm{obs}} + \Delta q \leq \langle q(\mathbf{r}) \rangle_{\mathbf{r}}
\end{aligned}
\tag{4}
$$

where Δq is a parameter separating the ranges of values of q for which V^{qr} is increasing quadratically and linearly with increasing q. Expression (4) represents an upper-bound restraint q^{obs} to $\langle q(\mathbf{r}) \rangle_{\mathbf{r}}$. A lower-bound restraint can be obtained by

replacing Δq by $-\Delta q$ and inverting the inequality symbols in (4). This is useful when treating the absence of a particular NOE signal in a NOESY spectrum as indicative of some minimum proton–proton distance (de Vlieg et al., 1986).

In most applications of structure refinement the ensemble average $\langle \ \rangle_{\mathbf{r}}$ in expression (4) is omitted, only the instantaneous value of $q(\mathbf{r})$ is restrained. This procedure ignores the ensemble character of the conformational distribution. It basically reduces the latter to one conformation, $\mathbf{r}_{\langle q \rangle}$, that may be very unrealistic (Figure 1). Due to the non-linear dependence of $q(\mathbf{r})$ on $\mathbf{r}$, the average of q over an ensemble of conformations will be different from the value of q calculated using the average of $\mathbf{r}$ over the ensemble, i.e.

$$\langle q(\mathbf{r}) \rangle_{\mathbf{r}} \neq q(\langle \mathbf{r} \rangle_{\mathbf{r}}). \tag{5}$$

As a consequence, there may be no simple structure that will fit all the experimental data simultaneously (Jardetzky, 1980; Nanzer et al., 1994). In addition, omitting the averaging $\langle \ \rangle_{\mathbf{r}}$ from V^{qr} will strongly reduce the mobility of the molecular system (Torda et al., 1990; Nanzer et al., 1995).

A better approach is to approximate the ensemble average $\langle q(\mathbf{r}) \rangle_{\mathbf{r}}$ by a time (trajectory) average (Torda et al., 1989) or by an average over different molecules (Scheek et al., 1989; Bonvin et al., 1994; Fennen et al., 1995). In MD simulations the use of the time average

$$\langle q(\mathbf{r}) \rangle_{\mathbf{r}} = \overline{q(t)} \equiv t^{-1} \int_0^t q(\mathbf{r}(t'))dt' \tag{6}$$

is the natural choice. Expression (6) is the true average of q, but is not suitable for deriving a restraining force from V^{qr} during a simulation: the rate of change of $\overline{q(t)}$ depends on the length of the averaging period t. This problem is avoided by building a decay into the summation over time with a characteristic decay time or memory relaxation time τ such that

$$\langle q(\mathbf{r}) \rangle_{\mathbf{r}} = \overline{q(t;\tau)} \equiv \left(\tau \left(1 - e^{-\frac{t}{\tau}} \right) \right)^{-1} \\ \int_0^t e^{-(t-t')/\tau} q(\mathbf{r}(t'))dt' \tag{7}$$

is used in (4). This approach has been successfully applied in structure refinement based on NMR (Torda et al., 1990; Torda et al., 1993) or X-ray (Schiffer et al., 1995) data. This conventional time-averaging refinement relies on employing a high-quality physical force field, because it introduces more conformational freedom for the molecule.

The use of (7) in (4) is not wholly satisfactory, because the average value $\overline{q(t;\tau)}$ of q by definition lags behind the instantaneous value $q(\mathbf{r}(t))$. The force due to the restraining function continues to be applied for some time after $q(\mathbf{r}(t))$ has become smaller than q^{obs}. This problem can be resolved by applying a penalty function force only when both $\overline{q(t;\tau)}$ and $q(\mathbf{r}(t))$ violate the bound q^{obs}. The simplest way to enforce this restraint is to use a biquadratic penalty function (Scott et al., 1998).

$$V^{qr}\left(\langle q(\mathbf{r}) \rangle_{\mathbf{r}}, q(\mathbf{r}(t)); q^{\mathrm{obs}} \right) = 0$$
if $\langle q(\mathbf{r}) \rangle_{\mathbf{r}} \leq q^{\mathrm{obs}}$
or $q(\mathbf{r}(t)) \leq q^{\mathrm{obs}}$

$$= \frac{1}{2} K_{bq}^{qr} \left(\langle q(\mathbf{r}) \rangle_{\mathbf{r}} - q^{\mathrm{obs}} \right)^2 \cdot \left(q(\mathbf{r}(t)) - q^{\mathrm{obs}} \right)^2$$
if $q^{\mathrm{obs}} \leq \langle q(\mathbf{r}) \rangle_{\mathbf{r}} \leq q^{\mathrm{obs}} + \Delta q$
and $q^{\mathrm{obs}} \leq q(\mathbf{r}(t)) \leq q^{\mathrm{obs}} + \Delta q$

$$= \frac{1}{2} K_{bq}^{qr} \left(\langle q(\mathbf{r}) \rangle_{\mathbf{r}} - q^{\mathrm{obs}} - \frac{1}{2}\Delta q \right) \cdot \Delta q \cdot \\ \left(q(\mathbf{r}(t)) - q^{\mathrm{obs}} \right)^2$$
if $q^{\mathrm{obs}} + \Delta q \leq \langle q(\mathbf{r}) \rangle_{\mathbf{r}}$
and $q^{\mathrm{obs}} \leq q(\mathbf{r}(t)) \leq q^{\mathrm{obs}} + \Delta q$

$$= \frac{1}{2} K_{bq}^{qr} \left(\langle q(\mathbf{r}) \rangle_{\mathbf{r}} - q^{\mathrm{obs}} \right)^2 \cdot \\ \left(q(\mathbf{r}(t)) - q^{\mathrm{obs}} - \frac{1}{2}\Delta q \right) \cdot \Delta q$$
if $q^{\mathrm{obs}} \leq \langle q(\mathbf{r}) \rangle_{\mathbf{r}} \leq q^{\mathrm{obs}} + \Delta q$
and $q^{\mathrm{obs}} + \Delta q \leq q(\mathbf{r}(t))$

$$= \frac{1}{2} K_{bq}^{qr} \left(\langle q(\mathbf{r}) \rangle_{\mathbf{r}} - q^{\mathrm{obs}} - \frac{1}{2}\Delta q \right) \cdot \Delta q \cdot \\ \left(q(\mathbf{r}(t)) - q^{\mathrm{obs}} - \frac{1}{2}\Delta q \right) \cdot \Delta q$$
if $q^{\mathrm{obs}} + \Delta q \leq \langle q(\mathbf{r}) \rangle_{\mathbf{r}}$
and $q^{\mathrm{obs}} + \Delta q \leq q(\mathbf{r}(t))$ \tag{8}

The corresponding lower-bound restraints can be obtained be replacing Δq by $-\Delta q$ and inverting

the inequality symbols in (8). If V^{qr} is to be used without the linearly increasing part, Eq. 8 reduces to

$$V^{qr}\big(\langle q(\mathbf{r})\rangle_{\mathbf{r}}, q(\mathbf{r}(t)); q^{\mathrm{obs}}\big) = 0$$
$$\text{if } \langle q(\mathbf{r})\rangle_{\mathbf{r}} \le q^{\mathrm{obs}}$$
$$\text{or } q(\mathbf{r}(t)) \le q^{\mathrm{obs}}$$

$$= \frac{1}{2} K_{bq}^{qr}\big(\langle q(\mathbf{r})\rangle_{\mathbf{r}} - q^{\mathrm{obs}}\big)^2 \cdot \big(q(\mathbf{r}(t)) - q^{\mathrm{obs}}\big)^2$$
$$\text{if } q^{\mathrm{obs}} < \langle q(\mathbf{r})\rangle_{\mathbf{r}}$$
$$\text{and } q^{\mathrm{obs}} < q(\mathbf{r}(t)). \tag{9}$$

Biquadratic time-averaged restraining (using Eq. 9 with upper bound as well as lower bound restraining) was applied to enforce ^3J-coupling constants towards the values measured for the peptide antamanide (Kessler et al., 1989), but the results were not very satisfactory (Scott et al., 1998). Therefore, we decided to investigate the particular difficulties of using ^3J-value restraints in structure refinement.

The vicinal ^3J-coupling constant $J(\theta)$ between two nuclei covalently linked by three bonds can be approximately expressed in terms of torsion angle θ between two planes defined by each nucleus and the two nuclei or atoms that constitute the covalent link to the other nucleus through the Karplus relation (1959)

$$^3J(\theta) = a\cos^2\theta + b\cos\theta + c \tag{10}$$

where a, b and c are constants that are calibrated empirically (de Marco et al., 1978; Pardi et al., 1984; Brüschweiler and Case, 1994; Wang and Bax, 1996; Schmidt et al., 1999). For peptides it is customary to express ^3J as a function of the ϕ-angle (C-N-C_α-C) or the χ_1-angle (N-C_α-C_β-C_γ),

$$\theta = \phi + \delta_\phi \tag{11}$$

and

$$\theta = \chi_1 + \delta_\chi. \tag{12}$$

The values of δ_ϕ and δ_χ depend on the local geometry of the peptide (L- or D-amino acid) and on the particular nuclei (protons) involved in the coupling (van Gunsteren et al., 1996a). The dependence of $^3J_{HN-H_\alpha}$ upon the backbone ϕ-angle is shown in Figure 2. The function $^3J(\phi)$ has the following characteristics:
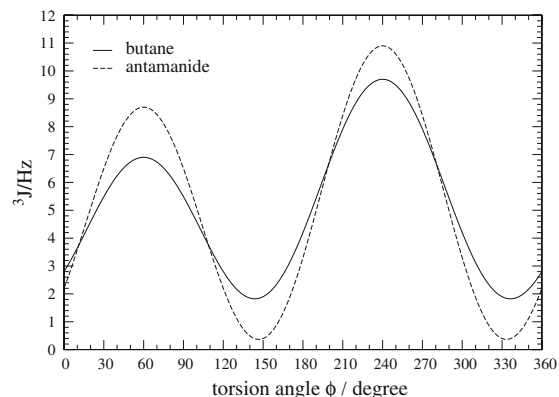

Figure 2. ^3J-coupling constant as function of a torsion angle ϕ. *solid line:* Karplus curve (Eq. 10) used for a torsion angle (θ) in butane but given as a function of the C_1-C_2-C_3-C_4-torsion angle (ϕ), ($a = 6.4$, $b = -1.4$, $c = 1.9$ (Pardi et al., 1984) and $\delta_\phi = -60°$), *dashed line:* Karplus curve for the H-N-C_α-H-torsion angle (θ) in antamanide but given as a function of the C-N-C_α-C angle (ϕ), ($a = 9.4$, $b = -1.1$, $c = 0.4$ (Bystrov 1976) and $\delta_\phi = -60°$).

1. Its inverse is multiple-valued, i.e. more than one ϕ-value is mapped onto one ^3J-value.
2. The gradient of $^3J(\phi)$ with respect to ϕ is varying substantially.
3. Its range of values is limited, some extreme ^3J-values are only reached for a few ϕ-values.

These characteristics cause problems when using ^3J-values directly in structure refinement, i.e. when setting $q = {}^3J$ in Eqs. (2–9). These problems are the subject of this article and their effects can be alleviated by the introduction of an oscillating factor $\cos^2(\omega^{qr}t)$ which during a period $\tau^{qr} = \frac{\pi}{\omega^{qr}}$ scales the torsion angle potential energy function V^{tors} and the restraining function V^{qr}

$$V(q(\mathbf{r})) = \cos^2(\omega^{qr}t)\cdot$$
$$\big[V^{\mathrm{tors}}(\mathbf{r}) + V^{qr}\big(\langle q(\mathbf{r})\rangle_{\mathbf{r}}, q(\mathbf{r}(t)); q^{\mathrm{obs}}\big)\big] \tag{13}$$

and thus permits the angle to cross over otherwise unsurmountable barriers. The oscillating factor is switched on as soon as the average ^3J-value deviates more than a certain threshold (ΔJ) from the target value. After one oscillating period is completed, the scaling is suspended for a time period (Δt_ω) that can be specified.

We demonstrate and analyse the effect of the various forms of penalty functions for a model system consisting of liquid butane, and then apply

them to the cyclic peptide antamanide for which experimental ^3J-values are available.

Materials and methods

^3J-values were calculated and compared for MD simulations that employ different types of ^3J-value restraining:

1. no restraining ($V^{qr} = 0$, NR),
2. quadratic instantaneous restraining (V^{qr} only depends on $q(\mathbf{r}(t))$, IR),
3. quadratic time-averaging restraining (Eqs. (4 and 7), TA),
4. biquadratic mixed instantaneous/time-averaging restraining (Eqs. (7–8), BTA),
5. oscillating biquadratic mixed instantaneous/ time-averaging restraining (Eqs. (7–8) with Eq. (13), OBTA).

Two molecular systems were considered. First, 512 butanes molecules in a cubic periodic box with edge lengths of 4.41 nm were simulated. The C_1-C_2-C_3-C_4 dihedral angle was used to define an artificial ^3J-coupling constant. The system was simulated at constant volume and at a constant temperature of 300 K. The temperature coupling constant was $\tau_T = 0.1$ ps (Berendsen et al., 1984) and the leap-frog integration time step was 2 fs. The GROMOS potential energy function (set 45A3) for aliphatic united-atom carbons was used (Schuler et al., 2001). For restraining methods employing time-averaging the memory relaxation time was set to $\tau = 5.0$ ps (Nanzer et al., 1995). Simulations employing OBTA were performed using $\omega^{qr} = 0.2\pi$ ps^{-1} (i.e. $\tau^{qr} = 5.0$ ps), $\Delta t_\omega = 5.0$ ps and a threshold of $\Delta J = 0.7$ Hz. Bond-lengths were kept rigid using the SHAKE algorithm with a relative precision of 10^{-4} (Ryckaert et al., 1977). The system was equilibrated for 100 ps and production periods covered 500 ps. Configurations were saved every 0.2 ps for analysis.

Antamanide is a cyclic decapeptide for which experimentally measured $^3J_{HN-H_\alpha}$-values are available (Kessler et al., 1989). Previous studies using instantaneous restraining have found no single conformation which could explain the ^3J-values measured (Kessler et al., 1988, 1989; Brüschweiler et al., 1991). It was previously used to test J-value restraining methodology (Torda et al., 1993; Scott et al., 1998). One antamanide molecule immersed in

3002 water molecules in a cubic periodic box with edge length 4.488 nm was simulated at constant volume and temperature, similarly to the butane system. The water was modeled using the SPC water model (Berendsen et al., 1981) and antamanide according to the GROMOS force field parameter set 45A3 (Schuler et al., 2001; Oostenbrink et al., 2004). For restraining methods employing time-averaging, the memory relaxation time was set to $\tau = 5.0$ ps (Nanzer et al., 1995). Simulations employing OBTA were performed using $\tau^{qr} = 1, 5$ and 25 ps, $\Delta t_\omega = 5.0$ ps and a threshold of $\Delta J = 0.7$ Hz. Equilibration covered 100 ps and sampling the next 400 ps. This system set-up differs from that in (Torda et al., 1993; Scott et al., 1998):

(i) Here solvent molecules are explicitly simulated, whereas in (Scott et al., 1998) their effect was mimicked by stochastic and frictional forces,
(ii) the factor $(1 - e^{t/\tau})$ was approximated by t/τ in (Scott et al., 1998), and
(iii) in Scott et al. (1998) an older set of force field parameters, set 43A1 (van Gunsteren et al., 1996a; Daura et al., 1998) was used.

All simulations were carried out using the GROMOS biomolecular simulation software (van Gunsteren et al., 1996a; Scott et al., 1999; Christen et al., 2005).

Results and discussion

Butane

The C_1-C_2-C_3-C_4-torsion angle (ϕ) of butane has been restrained to four different target values of the ^3J-constant using the Karplus relation (Eq.10) with arbitrarily chosen coefficients ($a = 6.4$, $b = -1.4$, $c = 1.9$ (Pardi et al., 1984)), $\delta_\phi = -60°$). Four different restraining methods were employed each with two different force constants in Eqs. 4 and 8 ($K^{qr} = 2.5$ kJ mol^{-1} Hz^{-2}, $K^{qr}_{bq} = 2.5$ kJ mol^{-1} Hz^{-4} and $K^{qr} = 5.0$ kJ mol^{-1} Hz^{-2}, $K^{qr}_{bq} = 5.0$ kJ mol^{-1} Hz^{-4}). Δq was set to infinity, i.e. the penalty function had no linear part. Table 1 shows the ^3J-constants that have been calculated from these simulations.

All methods succeed in restraining the ^3J-value to the desired target value with deviations up to 1.1 Hz. For the IR and TA method raising the force constant leads to an improvement of the results by

Table 1. Average ^3J-values corresponding to an arbitrary angle that is shifted by $\delta_\phi = -60°$ from the C_1-C_2-C_3-C_4 torsion angle in butane calculated from simulations employing the four different restraining methods (IR, TA, BTA, OBTA).

Restraining method	Force constant K^{qr} K^{qr} = kJ mol^{-1} Hz^{-2} or K^{qr}_{bq} = kJ mol^{-1} Hz^{-4}	Target value			
		$^3J_0$ = 2.0 Hz	$^3J_0$ = 4.0 Hz	$^3J_0$ = 6.0 Hz	$^3J_0$ = 8.0 Hz
IR	2.5	2.9 (0.7)	4.1 (0.9)	5.8 (0.9)	7.2 (0.9)
IR	5.0	2.6 (0.5)	4.0 (0.7)	5.9 (0.7)	7.4 (0.7)
TA	2.5	3.0 (1.0)	4.3 (1.6)	5.8 (1.8)	6.9 (1.1)
TA	5.0	2.7 (0.8)	4.2 (1.7)	6.0 (1.9)	7.2 (1.3)
BTA	2.5	2.7 (0.6)	4.2 (1.4)	6.2 (1.4)	7.4 (1.1)
BTA	5.0	2.6 (0.6)	4.2 (1.4)	6.2 (1.3)	7.5 (1.1)
OBTA	2.5	2.6 (0.6)	4.2 (1.4)	6.2 (1.4)	7.3 (1.1)
OBTA	5.0	2.6 (0.6)	4.2 (1.4)	6.2 (1.3)	7.4 (1.0)

Restraining potential energy functions were constructed using the Karplus relation (Eq. 10) with a = 6.4, b = -1.4, c = 1.9 (Pardi et al., 1984) and $\delta_\phi = -60°$, and two different force constants K^{qr} for each restraining method. Root-mean-square fluctuations are given between parentheses.

up to 0.3 Hz, whereas for BTA and OBTA a marginal improvement is observed. The known effect that IR severely reduces the fluctuation of the torsion angle is (to some extent) reflected in the rms fluctuations of the ^3J-values, which are smaller for IR than for all other methods. TA improves on this weakness, which is, however, bought by a slightly worse agreement of the ^3J-value with the target value (except for $^3J_0$ = 6 Hz). For the extreme ^3J-values $^3J_0$ = 2 Hz and $^3J_0$ = 8 Hz, BTA and OBTA succeed in bringing the average ^3J-value closer to the target value. For the average values of simulations with $^3J_0$ = 4 Hz and $^3J_0$ = 6 Hz that are already in close vicinity of the target value for TA, no further improvement is achieved.

The results can be divided into two groups. For simulations with $^3J_0$ = 4 Hz and $^3J_0$ = 6 Hz close agreement with the target value is achieved for any of the employed restraining methods ($\Delta^3 J \leq 0.3$ Hz). By contrast, for simulations that restrain to $^3J_0$ = 2 Hz or $^3J_0$ = 8 Hz the deviation never falls below 0.5 Hz. This observation is a consequence of the way the restraining function is constructed. In Figure 3 the internal potential energy of butane and that of the restraining functions for each of the target values are depicted. For $^3J_0$ = 4 Hz and $^3J_0$ = 6 Hz minima or ranges of low potential energy in the restraining function are found at about the same torsion-angle values as the minima of the physical potential energy function. Thus, adding these two functions leads to an overall energy function with minima that correspond to the target ^3J-values.

For $^3J_0$ = 2 Hz the situation is different. The Karplus-curve (see Figure 2) reaches ^3J = 2 Hz for values of approximately 134°, 154°, 337° and 346° of the C_1-C_2-C_3-C_4-torsion angle. For these angles we find slopes in the physical energy function and the minima of the combined functions will be shifted with respect to the minima of the restraining function. Consequently, the overall function favors angles that do not correspond to the target value of the ^3J-constant. This effect is amplified by the curved shape of the Karplus curve: small changes in torsion angle can lead to big changes in the ^3J-value.

The restraining function for $^3J_0$ = 8 Hz exhibits the same features. In addition to that, however, a second effect comes into play. The Karplus curve has two maxima (^3J = 6.9 Hz and ^3J = 9.7 Hz for these simulations, see Figure 2). The restraining function depends on the difference between the target value $^3J_0$ and the value of the Karplus curve at the current angle $^3J(\phi)$. Therefore, each target value that is higher than the lower of the two maxima will cause a minimum in the restraining function at the angle of this (lower) maximum. For $^3J_0$ = 8 Hz the minimum appears at about $\phi = 60°$ (see Figures 2 and 3). The fact that it restrains to a ^3J-value which is not the target value, is reflected in the small offset from zero at the minimum. The surrounding high barriers cause the angle to be trapped in the wrong minimum.

Both, the restraining function with $^3J_0$ = 2 Hz and the one with $^3J_0$ = 8 Hz exhibit exceptionally high barriers - an effect that occurs when the target value is close to an extremum of the Karplus curve.

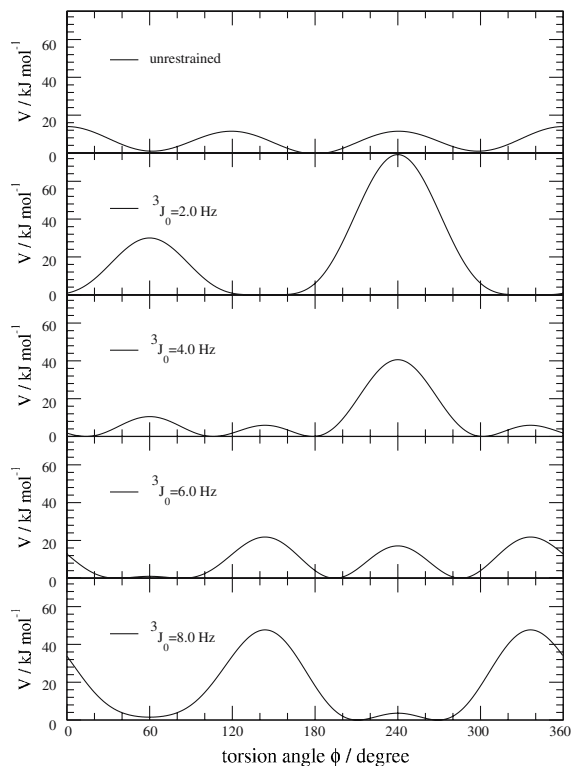*Figure 3.* Potential energy along a (restrained) torsional degree of freedom. Upper panel: $V^{phys}(\phi)$. Other panels: Potential energy term V^{qr} for butane as function of the C_1-C_2-C_3-C_4-torsion angle: (IR) restrained to $^3J_0 = 2.0$ Hz, $^3J_0 = 4.0$ Hz, $^3J_0 = 6.0$ Hz and $^3J_0 = 8.0$ Hz, respectively, using a Karplus curve with $a = 6.4$, $b = -1.4$, $c = 1.9$ (Pardi et al. 1984) and $\delta_\phi = -60°$ and a force constant $K^{qr} = 2.5$ kJ mol^{-1} Hz^{-2}.

Consider a high $^3J_0$-value, i.e. one that is close to a maximum. With the restraining function having as argument the squared difference between the target value and the ^3J-value that corresponds to the current angle, only a small increase in energy will occur for angle values around this maximum. On the other hand, for angles with ^3J-values far from this maximum of the Karplus curve large differences between the target value and the current ^3J-value will result and hence the restraining energy in these regions will be high. Lowering the resulting energy barriers by lowering the force constant will result in a loss of potential energy precision in regions with low energy barriers.

Figure 4 shows the distributions of the C_1-C_2-C_3-C_4-torsion angle of butane, which have been calculated from simulations, that have been restrained to $^3J_0 = 4.0$ Hz and to $^3J_0 = 8.0$ Hz, respectively. For an unrestrained simulation one would expect a high peak at 180° and two lower
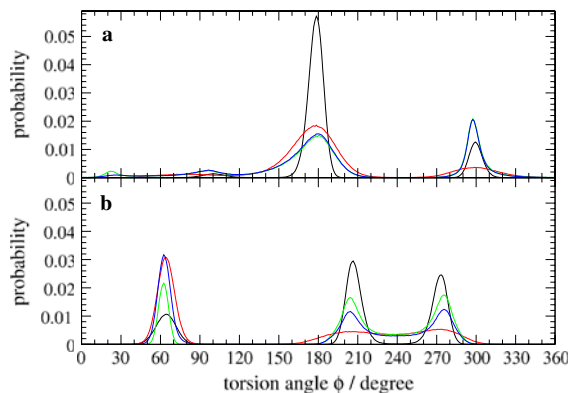

Figure 4. Probability distribution of the C_1-C_2-C_3-C_4-torsion angle ϕ in butane for four different ^3J-value restraining methods (IR: black, TA: red, BTA: green, OBTA: blue) a: restrained to $^3J_0 = 4.0$ Hz, b: restrained to $^3J_0 = 8.0$ Hz, force constant $K^{qr} = 5.0$ kJ mol^{-1} Hz^{-2} and $K^{qr}_{bq} = 5.0$ kJ mol^{-1} Hz^{-4}, respectively.

peaks at 60° and 300°, corresponding to one *trans*-conformation and two *gauche*-transformations of the C_1-C_2-C_3-C_4-torsion angle. The restraining function for $^3J_0 = 4$ Hz very much resembles the physical energy function and consequently distinct peaks appear at 180° and at 300°. The absence of a peak at 60° is due to the maximum at 60° in the restraining function. The sum of a maximum in the restraining function and a minimum in the physical energy function leads to two smaller, slightly shifted wells in the total energy function, which are reflected by small peaks in the angle distribution at about 30° and 100°. In Figure 4b ($^3J_0 = 8$ Hz) the restraining function clearly dominates the distribution. Peaks appear at the positions, where the restraining function has minima. For the peaks at 210° and at 270° the influence of the physical energy function is only perceivable through a slight shift to lower angles for the former peak and to higher angles for the latter peak. This effect is stronger for the methods that employ time-averaging than for instantaneous restraining. The third peak at around 60°, which is for most methods higher than the other two peaks (except IR), illustrates the effect of being trapped in the wrong minimum (see above). The minimum at $\phi = 60°$ in the restraining function, which restrains to a wrong ^3J-value, coincides with a minimum in the physical energy function. The resulting minimum in the total potential energy is obviously even more favorable than the minima that correspond to the desired ^3J-value.
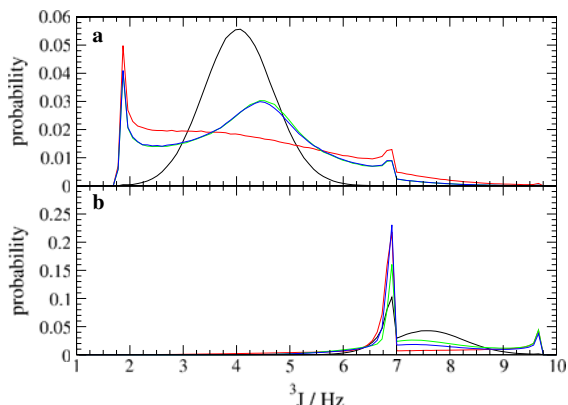
Figure 5. Probability distribution of ^3J-values in butane for four different restraining methods (IR: black, TA: red, BTA: green, OBTA: blue). a: restrained to $^3J_0 = 4.0$ Hz, b: restrained to $^3J_0 = 8.0$ Hz, force constant $K^{qr} = 5.0$ kJ mol^{-1} Hz^{-2} or $K^{qr}_{bq} = 5.0$ kJ mol^{-1} Hz^{-4}.

Figure 5 shows the ^3J-value distribution for the same simulations. For instantaneous restraining to $^3J_0 = 4.0$ Hz (black curve Figure 5a), the distribution is a broad peak centered at 4.0 Hz. The broadness of this peak, that seems to contradict the narrow peaks in the ϕ-distribution (Figure 4a), is a consequence of the Karplus curve. At $J = 4.0$ Hz this curve has steep slopes, i.e. small changes in ϕ will result in relatively big changes in ^3J-value and consequently, a narrow peak in the ϕ-distribution can correspond to a broad peak in the ^3J-distribution. For the methods based on time-averaging, the distributions look rather different. The central peak becomes even broader and is shifted to higher ^3J-values. This shift is counter-balanced by a peak at about 1.9 Hz and a small peak at 6.9 Hz appears. These ^3J-values correspond to two minima and a maximum in the Karplus curve and do not reflect a higher occurrence of the torsion angle at values that correspond to these ^3J-values. The following picture explains the situation: Suppose an angle passes with constant angular velocity through a region around one of the minima. Because the gradient of the Karplus curve is close to zero in that region, the ^3J-value changes little with the angle and in this case with time. This causes a peak in the distribution which is calculated from the time-series of the ^3J-values. This effect is not an artefact of the simulation, but should also occur in NMR measurements. For this reason alone, it is impossible to assign ϕ-values on the basis of ^3J-values. In the present case, the distributions of BTA and OBTA are almost indistinguishable, which is due to the fact that the scaling in OBTA is only switched on when the average of the ^3J-value differs more than 0.7 Hz from the target value.

Figure 5b ($^3J_0 = 8$ Hz) reveals a different situation. No or only a very broad and flat peak (in the case of IR) can be found in the vicinity of the target value $^3J_0 = 8.0$ Hz. Instead, we see for all methods a high and narrow peak centered at $^3J = 6.9$ Hz. Although, this ^3J-value corresponds to a maximum in the Karplus curve, this peak cannot entirely be explained by the above mentioned effect (the height of the peak in Figure 5a differs by a factor of 10 from that in Figure 5b). Rather, we see here a consequence of the fact that the angle can get trapped in a wrong minimum (see above) – a minimum that corresponds to the lower of the two maxima in the Karplus curve. At $^3J = 9.7$ Hz we see a small peak appear that corresponds to the second (higher) maximum. Judging from the height of the peak, this is the same type of effect we noticed in the upper part of the graph for the other extrema.

Antamanide

Six H-N-C_α-H-torsion angles (i.e. the corresponding ϕ-angles) have been restrained to reproduce their experimentally measured ^3J-constants. We used four different restraining methods (IR, TA, BTA, OBTA) each with three different force constants ($K^{qr} = 0.5$ kJ mol^{-1} Hz^{-2}, $K^{qr}_{bq} = 0.5$ kJ mol^{-1} Hz^{-4}, $K^{qr} = 2.5$ kJ mol^{-1} Hz^{-2}, $K^{qr}_{bq} = 2.5$ kJ mol^{-1} Hz^{-4} and $K^{qr} = 5.0$ kJ mol^{-1} Hz^{-2}, $K^{qr}_{bq} = 5.0$ kJ mol^{-1} Hz^{-4}). The OBTA method was applied with $\tau^{qr} = 5$ ps. This is an extension of previous work (Scott et al., 1998) in which the BTA restraining was introduced and was reported to result "in worse averages (residues 4, 6 and 9) and reduced fluctuations (residues 1, 5 and 10)". The results of our simulations are presented in Table 2.

For Residues 1, 5 and 6, the unrestrained (NR) simulations yield similar results as in Scott et al. (1998). We achieve much closer agreement with the experimental ^3J-constant for residues 9 and 10 ($\Delta J = 0.3$ Hz and $\Delta J = 0.5$ Hz compared to $\Delta J = 1.2$ Hz and $\Delta J = 1.3$ Hz in Scott et al. (1998)). For residue 4, however, our result deviates considerably more from the experimental value ($\Delta J = 4.1$ Hz

Table 2. Average ^3J-values corresponding to the six restrained H-N-C_α-H torsion angles in antamanide calculated from simulations employing the four different restraining methods (IR, TA, BTA, OBTA). For OBTA, $\tau^{gr} = 5$ ps.

Restraining method	Force constant K^{qr} = kJ mol^{-1} Hz^{-2} or K_{bq}^{qr} = kJ mol^{-1} Hz^{-4}	Val[1] $^3J_0$ = 7.3 Hz	Ala[4] $^3J_0$ = 8.6 Hz	Phe[5] $^3J_0$ = 6.8 Hz	Phe[6] $^3J_0$ = 6.6 Hz	Phe[9] $^3J_0$ = 8.3 Hz	Phe[10] $^3J_0$ = 6.7 Hz
NR		9.9 (1.5)	4.5 (2.6)	8.3 (0.6)	10.2 (1.3)	8.6 (2.2)	7.2 (2.1)
IR	0.5	9.4 (1.5)	6.9 (2.0)	8.4 (0.5)	9.8 (1.4)	8.1 (2.0)	8.1 (0.8)
IR	2.5	7.8 (1.1)	8.3 (1.0)	8.1 (0.7)	7.6 (1.1)	8.2 (1.0)	8.0 (0.7)
IR	5.0	7.6 (0.7)	8.4 (0.7)	7.8 (0.7)	6.8 (0.8)	8.2 (0.7)	7.7 (0.7)
TA	0.5	8.2 (3.0)	8.1 (2.3)	7.2 (2.2)	7.0 (3.6)	7.3 (2.8)	8.1 (1.0)
TA	2.5	7.5 (2.6)	8.5 (2.1)	7.0 (2.2)	7.5 (2.4)	8.3 (2.4)	7.0 (2.2)
TA	5.0	7.5 (2.7)	8.5 (2.0)	6.8 (2.4)	6.9 (2.6)	8.3 (2.2)	6.9 (2.1)
BTA	0.5	7.3 (1.5)	8.4 (0.5)	7.0 (2.4)	7.6 (1.8)	8.4 (2.3)	6.6 (2.1)
BTA	2.5	7.4 (2.6)	8.3 (0.5)	6.9 (2.5)	6.8 (2.7)	8.2 (1.6)	6.7 (2.2)
BTA	5.0	7.3 (2.4)	8.4 (0.8)	6.9 (2.8)	6.7 (2.8)	8.2 (0.7)	6.8 (2.5)
OBTA	0.5	8.2 (3.0)	8.3 (2.0)	7.0 (2.2)	7.4 (2.3)	8.3 (0.6)	7.2 (2.0)
OBTA	2.5	7.2 (2.1)	8.4 (0.4)	6.8 (2.5)	6.8 (2.5)	8.2 (2.2)	6.8 (2.4)
OBTA	5.0	7.3 (2.0)	8.3 (0.4)	6.8 (2.5)	6.7 (2.8)	8.3 (0.7)	6.9 (2.3)

Restraining potential energy functions were constructed using the Karplus relation (Eq. 10) with a = 9.4, b = −1.1, c = 0.4 (Bystrov 1976) and δ_ϕ = −60°, and three different force constants K^{qr} for each restraining method. Root-mean-square fluctuations are given between parentheses.

compared to $\Delta J = 1.2$ Hz). This may well be explained by the different simulation conditions.

Although ^3J-coupling constants can be measured with very high precision (better than ± 0.01 Hz), it is disputable whether the same precision criteria should be applied to averages calculated from molecular simulations. The parameters of the Karplus curve are generally determined by calibrating ^3J-constants measured in solution against the corresponding torsion angle derived from an X-ray structure (Pardi et al., 1984). It is difficult to numeralize the error introduced by the assumption that the angles in the crystal structure and in solution are the same and by the neglect of conformational dynamics. A comparison of the ^3J-values obtained using different sets of Karplus relation coefficients a, b and c showed a variation of up to 0.8 Hz (Peter et al., 2003). This suggests that the uncertainty in a ^3J-value calculated using the Karplus relation is of the order of 0.5 Hz.

In general, we see an improvement for almost all restraining methods and force constants. Exceptions are residue 10 (IR with all force constants, TA with a low force constant), residue 9 (TA with a low force constant) and residue 5 (IR, with a low force constant). Residues 9 and 10 already show reasonably good averages for the unrestrained simulations and thus, using IR or TA with a low force constant on angles that do not need much restraining is not advisable.

Inclusion of time-averaging yields improvement for Phe[5] and Phe[10]. The biquadratic functions (BTA and OBTA) show slightly better agreement with the target values than TA.

When considering ^3J-value fluctuations one has to be aware that the rms fluctuation of the ^3J-constant is only a very approximate measure for the fluctuations in the torsion angle, since J is not a linear function of ϕ. The rms fluctuations of the ϕ-angles which are presented along with the averages in Table 3 yield a more accurate picture of the atom mobility. In our work we generally find decreased ϕ-angle rms fluctuations (especially for high force constants) for IR and increased rms fluctuations for TA for both the ^3J-constant and the ϕ-angle. Both effects are expected and have been described before (Torda et al., 1993; Scott et al., 1998). From the rms fluctuations of the ^3J-values no clear trend as to whether BTA and OBTA increase or decrease the fluctuations can be distinguished. However, with the exception of Ala[4] and Phe[10] the rms fluctuation of the ϕ-angle increases considerably compared to NR for both methods using $K_{bq}^{qr} = 2.5$ kJ

Table 3. Averages and root-mean-square fluctuations of six restrained C-N-C_α-C torsion angles (in degrees) in antamanide calculated from simulations employing the four different restraining methods (IR, TA, BTA, OBTA).

Restraining method	Force constant K^{qr} K^{qr} = kJ mol^{-1} Hz^{-2} or K^{qr}_{bq} = kJ mol^{-1} Hz^{-4}	Val[1] $^3J_0$ = 7.3 Hz	Ala[4] $^3J_0$ = 8.6 Hz	Phe[5] $^3J_0$ = 6.8 Hz	Phe[6] $^3J_0$ = 6.6 Hz	Phe[9] $^3J_0$ = 8.3 Hz	Phe[10] $^3J_0$ = 6.7 Hz
NR		251 (15)	293 (26)	55 (13)	239 (16)	264 (18)	267 (46)
IR	0.5	258 (16)	278 (14)	56 (11)	241 (20)	267 (19)	51 (14)
IR	2.5	268 (18)	268 (12)	54 (14)	216 (26)	269 (13)	52 (15)
IR	5.0	275 (5)	270 (5)	52 (17)	280 (4)	271 (5)	49 (17)
TA	0.5	258 (32)	268 (20)	276 (16)	264 (39)	264 (35)	60 (22)
TA	2.5	184 (108)	258 (24)	278 (14)	228 (36)	261 (28)	276 (18)
TA	5.0	207 (99)	261 (22)	272 (40)	222 (37)	249 (56)	277 (16)
BTA	0.5	49 (30)	63 (11)	277 (19)	153 (85)	239 (70)	264 (35)
BTA	2.5	167 (97)	65 (11)	203 (99)	213 (49)	129 (101)	278 (20)
BTA	5.0	134 (106)	84 (63)	250 (56)	202 (74)	66 (15)	185 (105)
OBTA	0.5	256 (33)	266 (18)	276 (18)	218 (32)	67 (11)	277 (13)
OBTA	2.5	131 (94)	64 (11)	270 (44)	206 (27)	227 (82)	278 (19)
OBTA	5.0	100 (98)	63 (12)	244 (75)	205 (58)	71 (48)	150 (98)

For OBTA, τ^{qr} = 5 ps. Restraining potential energy functions were constructed using the Karplus curve with a = 9.4, b = −1.1, c = 0.4 (Bystrov 1976) and δ_ϕ = −60°, and three different force constants K^{qr} for each restraining method. Root-mean-square fluctuations are given between parentheses.

mol^{-1} Hz^{-4}. Solely, OBTA employed with the lowest force constant results in rms fluctuations which are of the same size as those observed in unrestrained simulations, for all six φ-angles.

These observations contradict previously published results [Scott et al. (1998)] which might partly be due to the use of higher force constants (K^{qr} = 10 kJ mol^{-1} Hz^{-2}, K^{qr} = 10 kJ mol^{-1} Hz^{-4}) therein.

The distribution of the restrained φ-angles in antamanide and the distribution of the corresponding ^3J-values are shown in Figures 6 and 7. All the restrained distributions differ from the unrestrained one. In general, methods using time-averaged restraining (TA, BTA and OBTA) sample the broadest range of φ-values, whereas IR severly restricts the region sampled. However, a narrow peak in the φ-distribution does, again, not necessarily result in a narrow peak in the ^3J-distribution. In almost all cases the restrained φ-distributions peak at other φ-values than the unrestrained ones. The dominating maxima in the ^3J-distribution are, however, those that are caused by the extrema of the Karplus curve (Val[1], Phe[6]). For Phe[10] the φ-distribution of IR has a maximum at 40°, whereas this distribution for TA has a maximum at 280°. Both angles approximately correspond to maxima in the Karplus curve which explains why their ^3J-distributions are very similar. The OBTA method samples the widest range of φ- and ^3J-values.

Table 4 shows the effect of varying the scaling period τ^{qr} of the OBTA method. The variation in average ^3J-values ranges from maximally 1.3 Hz for low K^{qr}_{bq} to maximally 0.3 Hz for large K^{qr}_{bq}-values.

Conclusion

The use of experimentally measured averages of observable quantities to derive the spatial "structure" or rather a most likely conformational distribution of biomolecules such as proteins and nucleic acids is not straightforward. In particular average ^3J-coupling constants measured in NMR experiments can hardly be used in structure refinement, because a ^3J-value is a multi-valued function of the corresponding torsional angle and this function, generally formulated in terms of a Karplus curve, has ranges with large $\frac{\partial J}{\partial \phi}$ derivative values. This makes it hardly possible to derive the characteristics of the torsional-angle distribution from the measured average ^3J-values.

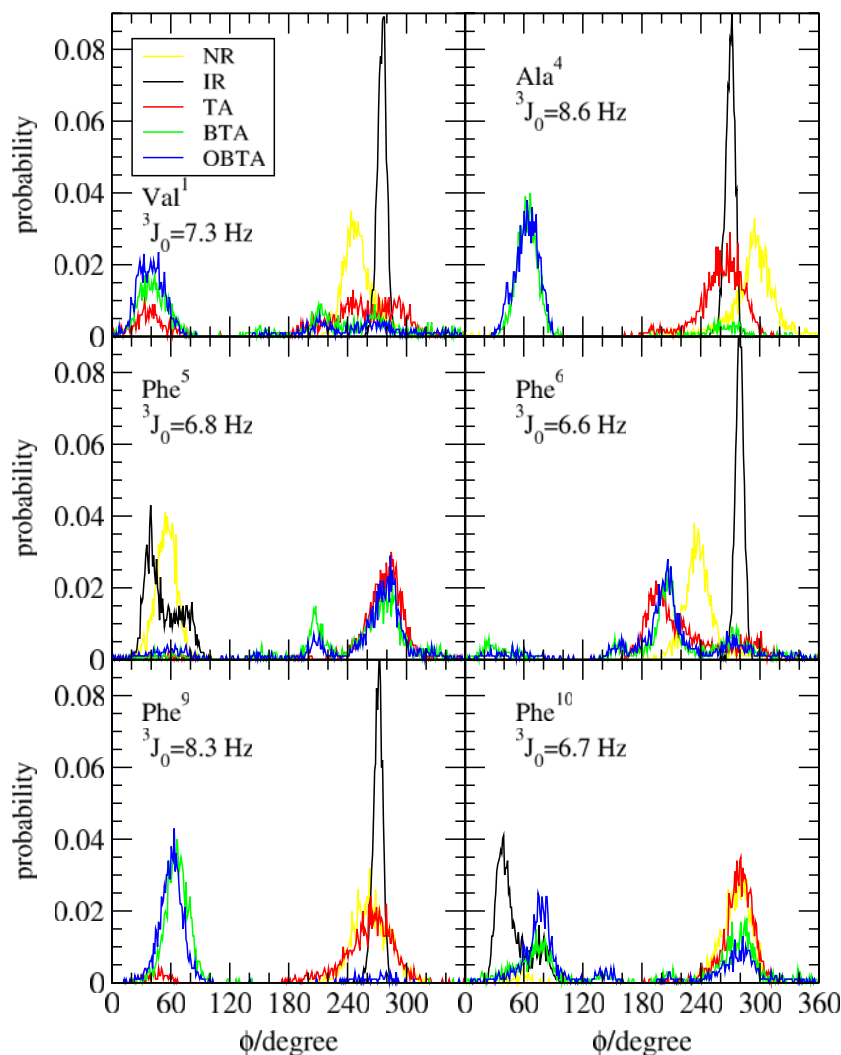Using a simple butane model system this problem was investigated. We performed MD

Figure 6. Distribution of the six restrained C-N-C_α-C-torsion angles in antamanide, *yellow:* unrestrained (NR), *black:* IR, *red:* TA, *green:* BTA *blue:* OBTA. Restraining functions were constructed using the Karplus relation (Eq. 10) with $a = 9.4$, $b = -1.1$, $c = 0.4$ (Bystrov 1976) and $\delta_\phi = -60°$ and a force constant of $K = 5.0$ kJ mol^{-1} Hz^{-2} and $K_{bq}^{qr} = 5.0$ kJ mol^{-1} Hz^{-4}, respectively. For OBTA, $\tau^{qr} = 5$ ps.

simulations with different penalty functions that restrain a particular ^3J-coupling constant to a preset target value $^3J_0$ and analysed the effects of the different types of restraining for different target values. A proper sampling of the torsional-angle degree of freedom becomes difficult for target $^3J_0$ values that are close to the extrema of the Karplus curve used in the calculations of the ^3J-value from the torsional angle. Because for $^3J_0$-values around the higher of the two maxima of the Karplus curve the relation between ^3J-value and torsion angle is straightforward, in

practice one may use torsion-angle restraining for these $^3J_0$-target values. For intermediate $^3J_0$-target values torsion-angle restraining restricts the sampling too much, so ^3J-value restraining including some form of time-averaging is the method of choice.

In order to enhance the sampling during the structure refinement MD simulations, introduction of an oscillating factor in the restraining penalty function was proposed. It temporarily scales down the torsional (V^{tors}) and restraining (V^{res}) potential energy for the torsion-angle degree
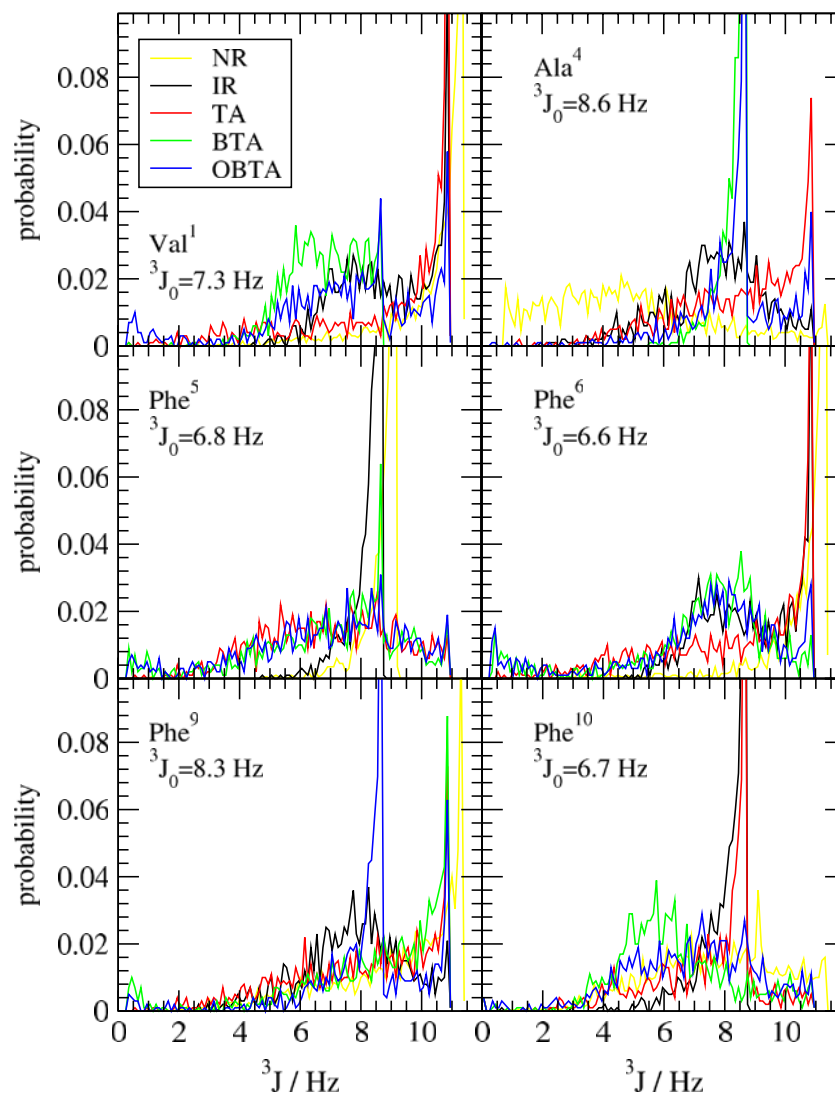
Figure 7. Distribution of the ^3J-values corresponding to the six restrained $H\text{-}N\text{-}C_\alpha\text{-}H$-torsion angles in antamanide, *yellow:* unrestrained (NR), *black:* IR, *red:* TA, *green:* BTA, *blue:* OBTA. Restraining functions were constructed using the Karplus relation (Eq. 10) with $a = 9.4$, $b = -1.1$, $c = 0.4$ (Bystrov 1976) and $\delta_\phi = -60°$ and a force constant of $K^{qr} = 5.0$ kJ mol^{-1} Hz^{-2} and $K_{bq}^{qr} = 5.0$ kJ mol^{-1} Hz^{-4}, respectively. For OBTA, $\tau^{qr} = 5$ ps.

of freedom when the average ^3J-value does not match the target ^3J-value. This allows the torsion angle to escape from the energy minimum in which it is (wrongly) trapped.

The cyclic decapeptide antamanide in aqueous solution was used to test the proposed restraining method and to compare its performance to that of other methods. The following conclusions could be drawn

1. Without any ^3J-value restraining (NR), the GROMOS 45A3 force field and explicit water

simulation used in the present work reproduce better the experimentally measured ^3J-values than the previously used (Torda et al., 1993; Scott et al., 1998) GROMOS 43A1 force field with stochastic solvent simulation.

2. Instantaneous restraining (IR) will enforce the target $^3J_0$-values onto the simulation, but at the price of a much too restrained torsion-angle distribution.

3. Time-averaging restraining (TA) (Torda et al., 1993) is a clear improvement over instanta-

Table 4. Average ^3J-values corresponding to the six restrained H-N-C_α-H torsion angles in antamanide from simulations employing the OBTA method.

Scaling factor τ^{qr}	Force constant K_{bq}^{qr} = kJ mol^{-1} Hz^{-4}	Val[1] $^3J_0$ = 7.3 Hz	Ala[4] $^3J_0$ = 8.6 Hz	Phe[5] $^3J_0$ = 6.8 Hz	Phe[6] $^3J_0$ = 6.6 Hz	Phe[9] $^3J_0$ = 8.3 Hz	Phe[10] $^3J_0$ = 6.7 Hz
NR		9.9 (1.5)	4.5 (2.6)	8.3 (0.6)	10.2 (1.3)	8.6 (2.2)	7.2 (2.1)
1 ps	0.5	8.1 (2.1)	8.2 (0.6)	7.6 (1.8)	7.5 (2.2)	7.9 (1.2)	8.0 (1.1)
5 ps	0.5	8.2 (3.0)	8.3 (2.0)	7.0 (2.2)	7.4 (2.3)	8.3 (0.6)	7.2 (2.0)
25 ps	0.5	7.7 (3.6)	8.5 (2.0)	6.9 (2.3)	7.6 (2.8)	8.4 (2.4)	6.8 (2.2)
1 ps	1.0	7.8 (1.9)	8.1 (0.7)	7.2 (1.6)	6.7 (1.9)	8.3 (0.6)	6.6 (2.1)
5 ps	1.0	7.2 (2.5)	8.5 (1.5)	7.0 (2.3)	7.3 (2.5)	8.4 (2.5)	6.8 (2.2)
25 ps	1.0	7.5 (3.5)	8.5 (2.0)	6.9 (2.5)	7.1 (2.8)	8.3 (2.5)	6.8 (2.3)
1 ps	2.5	7.5 (2.3)	8.3 (0.5)	7.2 (2.1)	6.9 (2.5)	8.3 (0.5)	6.8 (2.0)
5 ps	2.5	7.2 (2.1)	8.4 (0.4)	6.8 (2.5)	6.8 (2.5)	8.2 (2.2)	6.8 (2.4)
25 ps	2.5	7.2 (2.7)	8.2 (0.5)	6.9 (2.8)	6.6 (2.2)	8.2 (0.8)	7.0 (2.6)

Restraining potential energy functions were constructed using the Karplus curve with a = 9.4, b = −1.1, c = 0.4 (Bystrov 1976) and $\delta_\phi = -60°$, and three different force constants K^{qr} for each restraining method. Root-mean-square fluctuations are given between parentheses.

neous restraining, but generates too large variations in ^3J-values and torsion angles.

4. Biquadratic restraining (BTA) (Scott et al., 1998) based on both time-averaged and current ^3J-values alleviates this problem, but still suffers from torsion angles being trapped in spurious minima in the case of extreme $^3J_0$-target values.

5. Oscillating biquadratic restraining (OBTA) as proposed here alleviates the trapping problem by lowering the energy barriers temporarily if simulated and target ^3J-values do not match. It shows a wider sampling than the other restraining methods. In the antamanide example a restaining force constant of K_{bq}^{qr} = 2.5 kJ mol^{-1} Hz^{-4} with τ^{qr} = 5 ps yields optimal results in terms of reproduction of the target $^3J_0$-value by the ensemble averaged ^3J-value and the distribution of torsion angles.

6. Enforcing a ^3J-value on a torsion angle changes its conformational distribution and might affect the secondary structure of a polypeptide (especially when restraining H-C_α-C_β-H-torsion angles). Hence, for larger systems restraining method and force constant should possibly be adjusted individually for each restrained torsion angle.

We note that instead of scaling the potential energy function other methods may be used to drive a torsion angle away from values that yield the wrong ^3J-value. Here we think of the local-elevation search (Huber et al., 1994) or any other method that deforms the energy surface to enhance sampling (Christen and van Gunsteren (in press).

References

Berendsen, H.J.C., Postma, J.P.M., van Gunsteren, W.F. and Hermans, J. (1981) *Intermolecular Forces*, Reidel, Dordrecht, pp. 331–342.

Berendsen, H.J.C., Postma, J.P.M., van Gunsteren, W.F., Di Nola, A. and Haak, J.R. (1984) *J. Chem. Phys.*, **81**, 3684–3690.

Bonvin, A.M.J.J., Boelens, R. and Kaptein, R. (1994) *J. Biomol. NMR*, **4**, 143–149.

Brüschweiler, R. and Case, D.A. (1994) *J. Am. Chem. Soc.*, **116**, 11199–11200.

Brüschweiler, R., Blackledge, R. and Ernst, R.R. (1991) *J. Biomol. NMR*, **1**, 3–11.

Bystrov, V.F. (1976) *Prog. NMR Spectroscopy*, **10**, 41–81.

Case, D.A. (1998) *Encyclopaedia of Computational Chemistry*, Vol. 3, Wiley & Sons, Ltd. Chap. NMR Refinement, pp. 1866–1876.

Christen, M. and van Gunsteren, W.F. in press. *J. Comput. Chem.*

Christen, M., Hünenberger, P.H., Bakowies, D., Baron, R., Bürgi, R., Geerke, D.P., Heinz, T.N., Kastenholz, M.A., Kräutler, V., Oostenbrink, C., Peter, C., Trzesniak, D. and van Gunsteren, W.F. (2005) *J. Comput. Chem.*, **26**, 1719–1751.

Daura, X., Mark, A.E. and van Gunsteren, W.F. (1998) *J. Comput. Chem.*, **19**, 535–547.

de Marco, A., Llinas, M. and Wüthrich, K. (1978) *Biopolymers*, **17**, 617–636.

de Vlieg, J., Boelens, R., Scheek, R.M., Kaptein, R. and van Gunsteren, W.F. (1986) *Israel J. Chem.*, **27**, 181–188.

Fennen, J., Torda, A.E. and van Gunsteren, W.F. (1995) *J. Biomol. NMR*, **6**, 163–170.

Hendrickson, W.A. (1981) *Biomolecular Structure, Conformation, Function and Evolution, Volume I: Diffraction and Related Studies*, Pergamon, Oxford.

Huber, T., Torda, A.E. and van Gunsteren, W.F. (1994) *J. Comput.-Aided Mol. Design*, **8**, 695–708.

Jardetzky, O. (1980) *Biochim. Et Biophys. Acta*, **621**, 227–232.

Kaptein, R., Zuiderweg, E.R.P., Scheek, R.M., Boelens, R. and van Gunsteren, W.F. (1985) *J. Mol. Biol.*, **182**, 179–182.

Karplus, M. (1959) *J. Chem. Phys.*, **30**, 11–15.

Karplus, M. and McCammon, J.A. (2002) *Nat. Struct. Biol.*, **9**, 788–788.

Kessler, H., Bats, J.W., Lautz, J. and Muller, A. (1989) *Liebigs Annalen der Chemie*, **9**, 913–928.

Kessler, H., Griesinger, C., Lautz, J., Mueller, A., van Gunsteren, W.F. and Berendsen, H.J.C. (1988) *J. Am. Chem. Soc.*, **110**, 3393–3396.

Nanzer, A.P., Poulsen, F.M., van Gunsteren, W.F. and Torda, A.E. (1994) *Biochemistry*, **33**, 14503–14511.

Nanzer, A.P., van Gunsteren, W.F. and Torda, A.E. (1995) *J. Biomol. NMR*, **6**, 313–320.

Norberg, J. and Nilsson, L. (2003) *Quart. Rev. Biophys.*, **36**, 257–306.

Oostenbrink, C., Villa, A., Mark, A.E. and van Gunsteren, W.F. (2004) *J. Comput. Chem.*, **25**, 1656–1676.

Pardi, A., Billeter, M. and Wüthrich, K. (1984) *J. Mol. Biol.*, **180**, 741–751.

Peter, C., Rüping, M., Wörner, H.J., Jaun, B., Seebach, D. and van Gunsteren, W.F. (2003) *Chem.-A Eur. J.*, **9**, 5838–5849.

Ryckaert, J.P., Ciccotti, G. and Berendsen, H.J.C. (1977) *J. Comput. Phys.*, **23**, 327–341.

Scheek, R.M., van Gunsteren, W.F. and Kaptein, R. (1989) *Methods Enzymol.*, **177**, 204–218.

Schiffer, C.A., Gros, P. and van Gunsteren, W.F. (1995) *Acta Crystallographica D – Biol. Crystallogr.*, **51**, 85–92.

Schmidt, J.M., Blumel, M., Lohr, F. and Rüterjans, H. (1999) *J. Biomol. NMR*, **14**, 1–12.

Schuler, L.D., Daura, X. and van Gunsteren, W.F. (2001) *J. Comput. Chem.*, **22**, 1205–1218.

Scott, W.R.P., Mark, A.E. and van Gunsteren, W.F. (1998) *J. Biomol. NMR*, **12**, 501–508.

Scott, W.R.P., Hünenberger, P.H., Tironi, I.G., Mark, A.E., Billeter, S.R., Fennen, J., Torda, A.E., Huber, T., Krüger, P. and van Gunsteren, W.F. (1999) *J. Phys. Chem. A*, **103**, 3596–3607.

Torda, A.E., Scheek, R.M. and van Gunsteren, W.F. (1989) *Chem. Phys. Lett.*, **157**, 289–294.

Torda, A.E., Scheek, R.M. and van Gunsteren, W.F. (1990) *J. Mol. Biol.*, **214**, 223–235.

Torda, A.E., Brunne, R.M., Huber, T., Kessler, H. and van Gunsteren, W.F. (1993) *J. Biomol. NMR*, **3**, 55–66.

van Gunsteren, W.F. and Berendsen, H.J.C. (1990) *Angewandte Chemie-International Edition in English*, **29**, 992–1023.

van Gunsteren, W.F., Billeter, S.R., Eising, A.A., Hünenberger, P.H., Krüger, P., Mark, A.E., Scott, W.R.P. and Tironi, I.G. (1996a) *Biomolecular Simulation: The GROMOS96 Manual and User Guide*. Vdf Hochschulverlag AG an der ETH Zuerich, Switzerland.

van Gunsteren, W.F., Bonvin, A.M.J.J., Daura, X. and Smith, L.J. (1999) *Biological Magnetic Resonane: Volume 17: Structure Computation and Dynamics in Protein NMR*. Kluwer Academic/Plenum Publishers, New York. Chap. Aspects of Modeling Biomolecular Structure on the Basis of Spectroscopic or Diffraction Data, pp. 3–35.

van Gunsteren, W.F., Nanzer, A.P. and Torda, A.E. (1996b) (3–28 July) Molecular simulation methods for generating ensembles or trajectories consistent with experimental data. pp. 777–788 of: Binder, K. and Ciccotti, G. (Eds.), *Monte Carlo and Molecular Dynamics of Condensed Matter Systems, Proceedings of the Euroconference*, vol. 49.

Wang, A.C. and Bax, A. (1996) *J. Am. Chem. Soc.*, **118**, 2483–2494.